Potentialities and Criticalities of Flexible-Rate Transponders in DWDM Networks: A Statistical Approach

Mattia Cantono, Roberto Gaudino, and Vittorio Curri

***Abstract*—We propose a novel method to assess physical layer potentialities of core optical networks aimed at finding solutions that better exploit the installed equipment. We focus on the use of flexible-rate transponders for the implementation of the elastic paradigm on the state-of-the-art dense wavelength-division-multiplexed fixed-grid network scenarios. We make use of the waveplane-based routing and wavelength assignment algorithm presented in Dai et al. [J. Lightwave Technol., vol. 33, p. 3815, 2015] to implement a progressive statistical loading of the analyzed network topology, and perform a Monte Carlo analysis delivering a statistical characterization of the average bit rate per lightpath together with the assessment of network blocking. The proposed method allows for the identification of criticalities in terms of link congestion and lightpath quality of transmission, addressing solutions by identifying network bottlenecks. We apply the proposed method to a large pan-European network topology comparing two different transmission techniques for the implementations of flexible-rate transponders: *pure* PM-m-QAM versus hybrid modulation formats. Over this realistic network example, besides displaying the overall statistics for the average bit rate per lightpath, we show statistics for critical lightpaths and congested fiber links.**

***Index Terms*—Optical fiber communications; Optical fiber networks; Waveplane-based network performance analysis.**

I. Introduction

IP traffic is foreseen to grow at a compound annual growth rate of 23% from 2014 to 2019 [1], roughly corresponding to 2.8-fold growth in five years. According to [1], the increase of traffic generated by the final user will become dominant in the analyzed period 2014–2019 thanks to the diffusion of personal applications sharing data—mostly videos—on the Internet, enabled by the pervasive diffusion of broadband access technologies. Moreover, the traffic for the 60 busiest minutes of the day will experience a growth rate 20% higher than the average Internet traffic.

A similar scenario will strongly modify the traffic model for core transport networks, which will become more and more unpredictable and subject to serious variations with time. Therefore, such networks—besides growing as total transport capacity—will have to be responsive to relevant dynamic fluctuations of traffic demand. Hence, the implementation of the elastic network paradigm will be a firm and unpostponable request.

On the other hand, it should be considered that large telecommunications carriers intend to continue exploiting the already installed fibers roughly until 2025 [2]. Such a requirement is aimed at returning the large capital expenditure investments on fiber links made in the early 2000s [2]. Hence, core network operators are looking for solutions to maximize the aggregate bit rate on the already-used fiber links thanks to advanced modulation formats and coherent detection, enabling at the same time flexible network loading. First, they will optimize dense wavelength-division-multiplexed (DWDM) fixed-grid transmission with the newest and most performing flexible transponders being able to trade off the delivered data rate with the quality of transmission of the available lightpath. Then, after reaching capacity saturation on active fibers, they will start to selectively switch on available single-mode dark fibers by planning spatial division multiplexing (SDM), avoiding for the envisioned time-span the installation of SDM solutions based on multicore or multimode fibers. To pursue such results, an accurate assessment of potentialities and criticalities of the network physical layer is an indispensable task.

As the use of elastic transponders is a key technology for the implementation of the elastic paradigm in DWDM networks [3], in this paper we compare two different implementations of flexible transponders based on polarization-division-multiplexed M-QAM modulation formats. One transponders' family is able to switch between M-QAM constellations—*pure* formats—delivering quantized bit-rate values; the other considers the use of time-division hybrid modulation formats (TDHMFs) [4,5], enabling it to tune with continuity the bit rate, tailoring its value to the lightpath's (LP's) optical signal-to-noise ratio (OSNR). A more detailed description of these technologies can be found in [4–6].

To perform the aforementioned comparison, we propose an innovative approach that we call the Statistical Network Assessment Process (SNAP). This methodology starts from the waveplane-based routing and wavelength

Manuscript received January 4, 2016; revised May 2, 2016; accepted May 2, 2016; published June 3, 2016 (Doc. ID 256621).

The authors are with the Department of Electronics and Telecommunications, Politecnico di Torino, Torino, Italy (e-mail: mattia.cantono@polito.it).

http://dx.doi.org/10.1364/JOCN.8.000A76

assignment (RWA) [6,7] and performs a progressive load of the network through a Monte Carlo analysis [8], in which the order according to which lightpath demands are served is varied. SNAP applies to both static and dynamic traffic models, and, in this paper, it is used for a static traffic scenario, i.e., with demands of infinite duration. The core concept of this method is to analyze a progressive random load of traffic to an optical network and to evaluate its performance under such random traffic conditions. The network can be completely unloaded at the beginning of the process—as it is in this work—or can carry some existing traffic. In our analysis, we consider networks operating according to the locally optimized globally optimized (LOGO) optimization strategy [9,10], meaning that each link runs at its optimal power [11,12]. Given the network topology graph, each fiber link is weighted by a quality of transmission (QoT) metric, the optical *noise-to-signal* ratio accumulation, computed by means of the incoherent Gaussian noise (GN) model [11]. This QoT cost is used during the network-loading phase for routing purposes and to determine the maximum bit rate at which each lightpath can operate for a given modulation strategy. Operating on a detailed description of the network topology, SNAP is able to estimate the statistics of the average bit rate per lightpath $R_{b,\lambda}$ for all possible lightpath demand arrangements. It also evaluates the network blocking performances, defined here as the ratio between the number of blocked demands over the total number of lightpath demands. Moreover, it statistically determines the criticalities of the physical layer as, for instance, the congestion of node-to-node links or the critical QoT in lightpaths. Such statistical characterization of critical aspects can be fruitfully used to derive general and statistically effective solutions. The knowledge of the full statistics of network metrics leads to useful insights into network performance. For example, the statistics of the average bit rate per LP, obtained through SNAP, can be used to assess the goodness of heuristics algorithms aimed at throughput maximization. In particular, one could easily state in which percentile of the distribution the average bit rate per LP obtained with the considered heuristics falls. In addition to this, one could also assess statistically network-striking features. For example, using SNAP may deliver the probability for the spectrum of a link to be utilized over a certain percentage, given some traffic, RWA, topology, and physical layer characteristics. Although Monte Carlo-based algorithms for network analysis have been frequently used in the past [6,13,14], the statistical interpretation of network metrics is a novel approach, to the best of our knowledge.

We remark that the proposed method is not aimed at providing optimal routing and wavelength solutions for a given traffic matrix and network topology; instead, it addresses the statistical benchmarking of the physical layer on a reconfigurable optical network scenario to identify its strengths and weaknesses under a random progressive traffic load.

Using SNAP, we compare the two considered flexible-rate transponder technologies on a pan-European network topology. We show that TDHMFs enable a capacity enhancement of 23% at a target pre-forward error correction (FEC) bit error rate (BER) level of $4 \cdot 10^{-3}$ with respect to *pure* formats, independently of the characteristic of the RWA algorithm considered in this paper. Moreover, we prove the importance of correctly modeling nonlinear fiber propagation to properly estimate network performance. In particular, we consider as a nonlinear propagation effect the generation of a noise-like disturbance called nonlinear interference (NLI) [11,15–23].

On the analyzed topology, we also show detailed results on link congestion and suggest possible general remedies to these criticalities.

The paper is organized as follows. Section II is devoted to describing the SNAP algorithm. Section III shows the use of SNAP to perform the comparison between pure and hybrid modulation approaches. In Section IV, the pan-European network scenario chosen for the comparison is described. Finally, results are shown and commented on in Section V, and, in Section VI, conclusions are made.

II. SNAP: Statistical Network Assessment Process

In this section, we introduce the Statistical Network Assessment Process. SNAP is an algorithm to statistically characterize the strengths and weaknesses of the physical layer in reconfigurable optical networks, and it is here applied to compare hybrid to pure modulation strategies for the implementation of flexible-rate transponders.

In this paper, we use the following network terminology. We refer to lightpaths as transparent optical connections between nodes not directly connected by fiber links. We suppose that network nodes include the equipment responsible for traffic loading and retrieving, and for transparent wavelength routing. Optical amplification at each output port of each node is included to recover for the loss experienced by lightpaths transparently routed, and to set the optimal power per channel on the output link. We define fiber links as the connections between two nodes. Fibers between nodes are in pairs, providing bidirectional connectivity between the nodes such that the network is considered as an undirected graph. Each fiber link is made by a cascade of identical spans. Each span is made of fiber followed by an erbium-doped fiber amplifier (EDFA), fully recovering its loss.

The flow chart of Fig. 1 describes the proposed algorithm. SNAP makes use of the following input information:

1) A set of node-to-node lightpath demands organized in a matrix fashion. Each element of the matrix $D_{i,j}$ represents the number of lightpaths to be allocated between node i and node j. While SNAP can work with any $D_{i,j}$ matrix, in Section IV we will focus on $D_{i,j} = 1 \forall i,j$ and $D_{i,j} = 0$ for $i = j$, i.e., one lightpath request for each node pair. Since we aim at analyzing the potentialities of the physical layer of a fully reconfigurable optical network, we consider demands expressed in terms of the number of requested lightpaths and not in terms of data rate.
2) A full description of the network topology and the characteristics of the physical layer (e.g., fiber type,

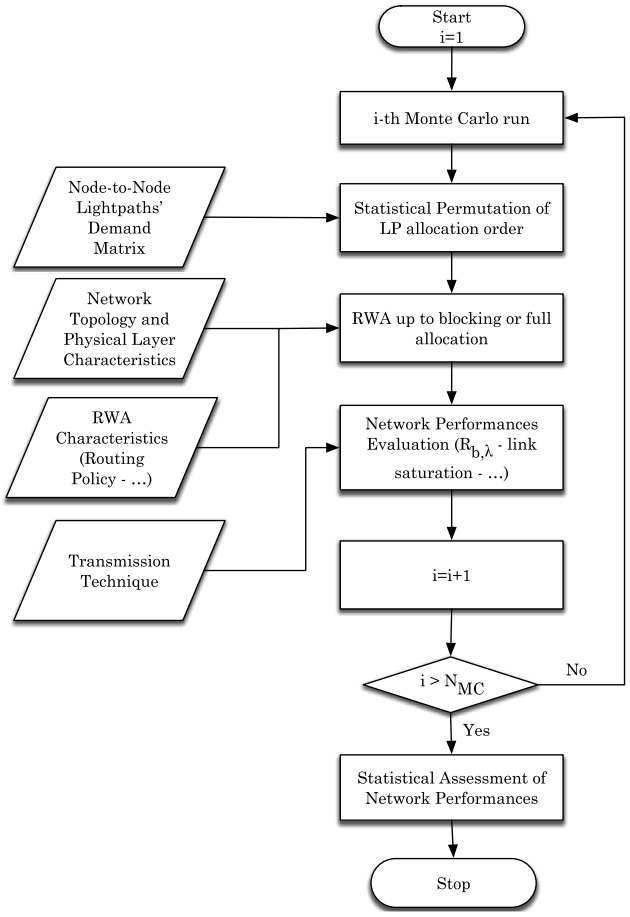

Fig. 1. Flowchart of the SNAP algorithm.

amplification method, slot size, number of channels, etc.). The physical layer parameters can be used to compute the figure of merit for the QoT of each lightpath, i.e., its OSNR. To do so, several nonlinear propagation models can be used, e.g., [11,15–23]. As will be described later on, in our analysis we exploit the incoherent GN model [11].

3) The characteristics of the RWA algorithm, such as the routing policy, namely, the way in which fiber paths between node pairs are computed and ranked. For example, a shortest link or smallest number of hops ranking could be adopted.
4) The transmission technique (e.g., pure or hybrid modulation formats) to determine the maximum allowable bit rate of each LP given its OSNR and the related pre-FEC target BER.

Given this information, a Monte Carlo analysis is performed. During each Monte Carlo run, a progressive load of the network takes place: the set of node-to-node ligthpath demands is randomly shuffled to vary the order in which requests are allocated. It should be highlighted that, in general, such a progressive network load can be executed on top of any existing network loading status. In this paper, we consider a fully unloaded network. In each Monte Carlo run, given the randomly ordered list of connection, an RWA process starts. The RWA process tries to allocate each LP request according to some user-defined policies (e.g., the routing strategy). To do so, optically transparent paths able to accommodate the considered LP demands are searched across the network. In our analysis, we make use of an RWA based on the waveplane method [6,7] to be fully described in Section III, but in general any RWA can be used. The RWA process terminates when the complete set of demands has been considered. Depending on the traffic and network topology characteristics, the RWA process may successfully allocate all demands, or some network blocking may occur.

After the completion of the allocation process, several network-performance metrics are computed for the ith Monte Carlo run. These may include the following:

- Average bit rate per lightpath $R^i_{b,\lambda}$ that is given by

$$R^i_{b,\lambda} = \frac{1}{N_{L,i}} \sum_{j=1}^{N_{L,i}} R_{b,j}[\text{Gbps}], \tag{1}$$

  where $N_{L,i}$ is the number of allocated lightpaths during the ith Monte Carlo run and $R_{b,j}$ is the bit rate of the jth LP.
- Spectral saturation of each fiber link, i.e., the details about channel occupation of each node-to-node fiber connection.
- Blocking information such as the number of blocked demands for each node or link.

The set of metrics to be considered can be modified in order to target specific alternative network aspects. In this sense, SNAP can be easily extended, providing a relevant flexibility in the characterization process. Due to the random scrambling of the set of input LP demands, the allocation process of each Monte Carlo run may differ from the one of the previous runs, and thus the output results of each run will generally be stochastic.

After the maximum number of Monte Carlo iterations N_{MC} has been reached, each metric can be statistically characterized with respect to the random allocation process of LPs. This means that the probability density function (PDF) of each analyzed metric can be derived, thus obtaining a *statistical* insight into network capabilities and critical aspects.

III. Physical Impairment Model and Routing Strategies

This section gives a detailed description of the nonlinear modeling and RWA options adopted in this paper.

In order to compare performances of time-division hybrid and pure modulation formats in a fixed-grid network scenario, the SNAP algorithm has been properly customized. In particular, we use the incoherent GN model [11] to evaluate propagation performance and a modified waveplane method [6,7] with QoT-based routing to perform RWA. The incoherent GN model is suitable for

impairment-aware networking scenarios, thanks to its independence from modulation formats and its modest computational cost. It has some limitations, e.g., for low-loss spans, but in general it has been proven to be sufficiently reliable for networking studies [8].

A fully transparent optical network with uniform links in terms of fiber and EDFA types has been assumed. We consider each node to be equipped with a colorless, directionless, and contentionless reconfigurable optical add–drop multiplexer (ROADM) [24–26]. Each fiber span is assumed to operate at its optimal power that is computed by means of the incoherent GN model as the LOGO principle prescribes [9,10], assuming full spectral load in each link. Moreover, all node-to-node links are supposed to be made by a cascade of amplified fiber spans. Consequently, the network may be represented as an undirected graph whose edges, the fiber links, are weighted by inverse OSNR (IOSNR) accumulation Δ_{IOSNR} that includes both the amplified spontaneous emission (ASE) noise introduced by the amplifiers and the NLI disturbance by the fiber propagation. We consider as reference bandwidth for the OSNR the LP bandwidth B_{ch}. Δ_{IOSNR} is additive span-by-span, and can be computed by means of the incoherent GN model [11]. In particular,

$$\Delta_{\mathrm{IOSNR}} = \frac{P_{\mathrm{ASE}}}{P_{\mathrm{ch}}} + \eta P_{\mathrm{ch}}^2, \tag{2}$$

where P_{ASE} is the ASE noise power in B_{ch} while P_{ch} is the power per channel, whose optimal value is given by

$$P_{\mathrm{ch,opt}} = \sqrt[3]{\frac{P_{\mathrm{ASE}}}{2\eta}}. \tag{3}$$

Here, η is the so-called NLI efficiency and depends on fiber parameters, total occupied bandwidth B_{opt}, number of channels N_{ch}, channel bandwidth B_{ch}, and the DWDM spacing Δf. We consider η in its worst case, i.e., for the center wavelength and referring to full spectral load. Such an assumption is reasonable and does not cause large overestimation in link QoT due to the weak dependence between η and the occupied bandwidth. Interested readers may refer to [8,10–12] for further details.

Given the IOSNR degradation introduced by each fiber span, it is possible to compute the OSNR of a lightpath propagating over N_f fiber links, with the jth link made of $N_{s,j}$ uniform spans, each of which introduces an IOSNR increase/degradation $\Delta_{\mathrm{IOSNR},j}$ by considering

$$\mathrm{OSNR}_{\mathrm{TOT}} = \mathrm{IOSNR}_{\mathrm{TOT}}^{-1} = \left[\sum_{j=1}^{N_f} (N_{s,j}\Delta_{\mathrm{IOSNR},j})\right]^{-1}. \tag{4}$$

Exploiting the additive property of IOSNR, it is possible to rank different lightpaths over an optical network graph, based on their QoT, that is directly related to the OSNR. In particular, the lightpath between two nodes having minimum $\mathrm{IOSNR}_{\mathrm{TOT}}$ will have the largest $\mathrm{OSNR}_{\mathrm{TOT}}$, and hence the best QoT. Based on this, it is possible to define a QoT-based routing algorithm for optical networks, according to which lightpaths are ranked based on their QoT. The IOSNR degradation term can be used to weight edges in the optical network graph. Standard graph algorithmic techniques can be used to compute the best QoT paths between node pairs. The OSNR computed by means of Eq. (4) can then be used to determine the maximum bit rate at which a lightpath can operate given the modulation strategy (hybrid or *pure*) and the selected target BER.

As an RWA strategy, we adopt a modified version of the so-called waveplane method [6] that makes use of the aforementioned QoT-based routing. The main idea of this method is to consider the network graph as a multigraph made of N_{ch} graphs, called *waveplanes*, where N_{ch} is the number of available wavelengths (λs). In waveplanes, each edge of the graph corresponds to a single λ on the corresponding fiber link. The waveplane-based method for RWA works as follows:

1) For each demand to be allocated, waveplanes are scanned to find a suitable working lightpath to accommodate the request.
2) Whenever a demand is allocated, the edges of the waveplane over which that demand was accommodated are removed from the waveplane itself. When all links are fully saturated, all waveplanes are empty.
3) If a demand cannot be allocated, it is flagged as blocked and the process moves to the following demand.

Unlike the original waveplane method [7], paths between a node pair are computed by using a k-shortest-path algorithm in which the best k_{MAX} paths in terms of QoT, i.e., lowest IOSNR degradation, are considered suitable paths for LPs. In particular, the term k_{MAX} represents the number of different paths between node pairs that can be used to find available wavelengths to accommodate LP demand routes. In this sense, the adopted RWA can be classified as a first-fit wavelength assignment with routing based on a k-shortest-path, best QoT routing policy. The use of a QoT-based routing policy allows for the allocation of demands on the highest available QoT path between a pair of nodes, thus maximizing the bit rate per LP, given the network loading.

We remark that the waveplane method for RWA was originally introduced as a heuristic RWA algorithm to find close-to-optimum RWA solutions for a given topology and set of traffic demands. To do so, a few randomly shuffled demand sequences are considered, and the realization which maximizes a given performance metric (e.g., the total network bit rate) is selected as the solution of the RWA problem [6]. Within SNAP, we apply it in a Monte Carlo analysis, aiming at characterizing the statistics of potentialities and criticalities of the physical layer on a reconfigurable optical network scenario. Thus, we consider a much larger set of randomly shuffled sequences, and we use the output of each RWA process to build the *statistics* of a set of network performance metrics of interest, so as to obtain results that are *independent* of the order in which LP demands are considered and thus as general as possible.

IV. Analysis of the Pan-European Network Topology

We tested the proposed algorithm on a realistic pan-European network topology obtained from the EU project IDEALIST [27]. The considered topology has 49 nodes and 68 bidirectional fiber links, and it is depicted in Fig. 2. We assume uniform links in terms of fiber and EDFA types. We consider standard single-mode fiber with the following characteristics: loss coefficient $\alpha_{\mathrm{dB}} = 0.2$ dB/km, dispersion coefficient $D = 16.7$ ps/nm/km, effective area $A_{\mathrm{eff}} = 80\ \mu\mathrm{m}^2$, and nonlinear index coefficient $n_2 = 2.5 \cdot 10^{-20}\ \mathrm{m}^2/\mathrm{W}$ corresponding to a nonlinear coefficient $\gamma = 1.27$ l/W/km. We suppose that all network ROADMs introduce a routing loss of 10 dB that is fully recovered with an additional EDFA at the output of the nodes. We do not consider any further impairment caused by cascaded filtering effect on channel spectra caused by ROADMs. All EDFAs have a 5 dB noise figure. Span lengths are not uniform across the network but are given directly from the topology data obtained from [27].

We assume that the transmission level operates on the C-band set to $B_{\mathrm{opt}} = 4$ THz and on the 50 GHz ITU-T grid, enabling a maximum of $N_{\mathrm{ch}} = 80$ lightpaths—wavelengths—per fiber. The network elasticity on this scenario is given by adopting flexible-rate transponders using multilevel modulation formats. We consider either elastic transponders based on pure formats—polarization multiplexed M-QAM—or on TDHMFs [4,5]. In both cases, the spectral efficiency varies from 2 to 12 bits per symbol (bpS), i.e., cardinality of modulation formats may adaptively grow from 2^2 (PM-BPSK) up to 2^{12} (PM-64-QAM). However, the delivered spectral efficiency versus the available OSNR is discrete when pure formats are used, whereas it is continuous for flexible-rate transponders based on TDHMF.

We consider modulation formats operating at gross symbol rate $R_{s,g} = 32$ GBaud per channel, corresponding to a net symbol rate $R_s = 25$ GBaud per channel due to protocol and coding overhead. We assume that the channels operate at pre-FEC BER $\leq 4 \cdot 10^{-3}$. Such a pre-FEC BER level is not referred to any specific standard or commercial product, as it has been selected to derive *reasonable* quantitative results. Considering specific FEC implementations, larger values of pre-FEC BER could be considered.

First, we verified the convergence of the Monte Carlo analysis, i.e., the number of Monte Carlo iterations N_{MC} needed to obtain statistically stable results. To this purpose, we consider the PDF of the average bit rate per LP given by Eq. (1) obtained with $N_{\mathrm{MC}} = 10^3$ and $N_{\mathrm{MC}} = 5 \cdot 10^4$. Results reported in Fig. 3 are obtained considering TDHMF and selecting as feasible paths between two nodes only the path having the largest OSNR, i.e., $k_{\mathrm{MAX}} = 1$.

We allocated symmetrically a single LP for each node pair, i.e., $D_{i,j} = 1 \forall i,j$ and $D_{i,j} = 0$ for $i = j$. In Fig. 3, a Gaussian fit for the two PDFs is also reported, showing good agreement with the simulative results. Therefore, a first result of the analysis is that the average bit rate per lightpath is Gaussian-distributed with respect to the lightpaths' allocations, and its average value can be used as a figure of merit of different implementations of the network physical layer. The PDF of $R_{b,\lambda}$ converges toward a truncated Gaussian due to the central limit theorem. $R_{b,\lambda}$ is in fact computed by summing a large set of random bit rates that, for TDHMF, are distributed almost uniformly in the interval [50 Gbps, 300 Gbps].

From Fig. 3, it is intuitive to understand that independently of the order in which LP demands are allocated, the considered network topology is able to deliver on average 211 Gbps per LP. This means 4.4 bpS per polarization, which is a value larger than the one delivered by a PM-16-QAM modulation format. We also remark that the variance of $R_{b,\lambda}$ is strictly related to the network blocking. In particular, since the complete set of LP demands cannot be allocated, the set of blocked LP demand will differ in each Monte Carlo run, and so the quantity $R_{b,\lambda}$ will be stochastic. Under the same test conditions, in particular $k_{\mathrm{MAX}} = 1$, if the physical layer was able to allocate all requests, the variance of $R_{b,\lambda}$ would be zero. This happens because all

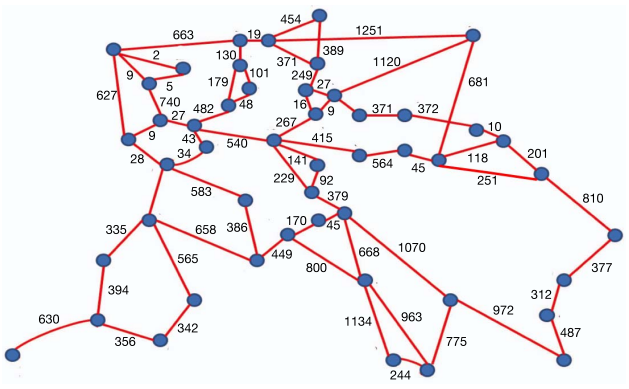

Fig. 2. Pan-European network topology. Edge labels are the lengths of each fiber pair in km.

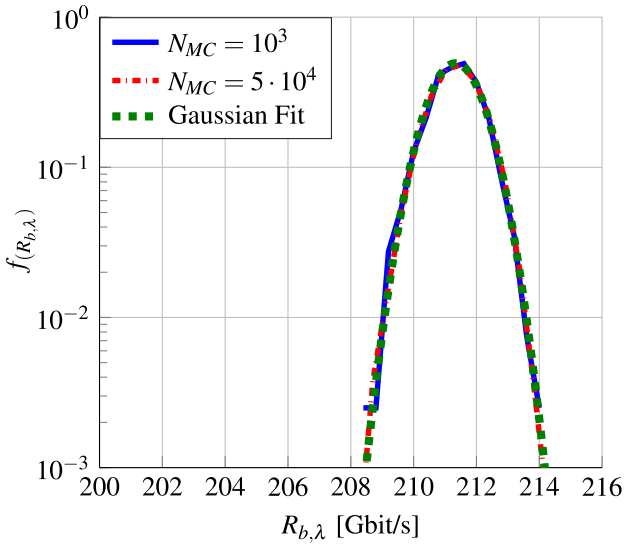

Fig. 3. Convergence of PDF of average bit rate per LP obtained considering TDHMF and $k_{\mathrm{MAX}} = 1$.

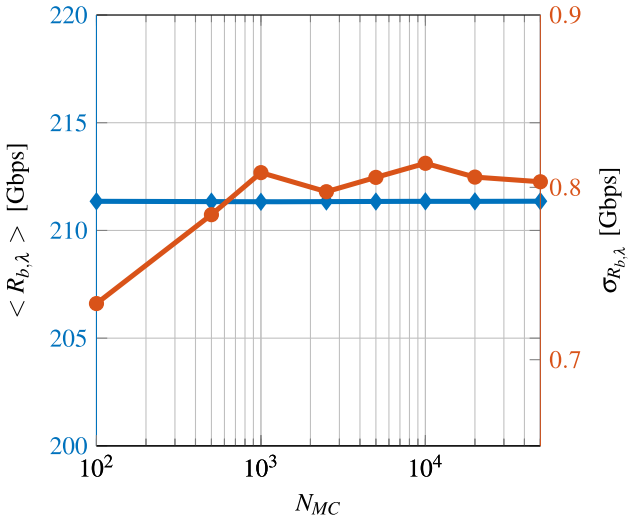

Fig. 4. Convergence of the mean value (left axis, diamond markers) and standard deviation (right axis, circular markers) of average bit rate per LP obtained considering TDHMF and $k_{\text{MAX}} = 1$.

possible LP requests would be allocated on the best OSNR path, thus giving a deterministic $R_{b,\lambda}$. Increasing the set of feasible paths, i.e., increasing k_{MAX}, expands the variability of the overall allocation process, thus increasing the variance of $R_{b,\lambda}$. Thus, in general, the stochastic behavior of $R_{b,\lambda}$ is caused by two factors: network blocking and routing strategy ($k_{\text{MAX}} > 1$).

In addition to the PDF of $R_{b,\lambda}$, we report in Fig. 4 its mean and standard deviation—indicated as $\langle R_{b,\lambda} \rangle$ and $\sigma_{R_{b,\lambda}}$, respectively—versus N_{MC}. It can be noted that the mean value of the average bit rate per LP already converges for $N_{\text{MC}} \geq 100$, whereas the standard deviation converges for $N_{\text{MC}} \geq 1000$. Hence, in order to obtain results presented in the next section, we safely set $N_{\text{MC}} = 2500$.

V. Results and Discussion

We applied the SNAP algorithm to the pan-European network scenario described in Section IV, considering the two transmission techniques operating the flexible-rate transponders described in Section I. The pure format approach considers elastic transponders able to select the highest-cardinality squared constellation from PM-BPSK up to PM-64-QAM, thus allowing a discrete tuning in data rate versus OSNR performances. On the other hand, TDHMF allows for the tuning of such characteristics with continuity. For the pure-format approach, we considered the formats most commonly used in coherent transceivers, i.e., the ones that are able to be used with threshold-based receivers. Although flexible transceivers, including PM-8-QAM, can be implemented by increasing the DSP complexity, we do not consider such a modulation format in our study. Moreover, nonsquared constellations are not uniquely defined, e.g., star-8-QAM versus rectangle-8-QAM [28], thus introducing additional degrees of freedom to the network analysis.

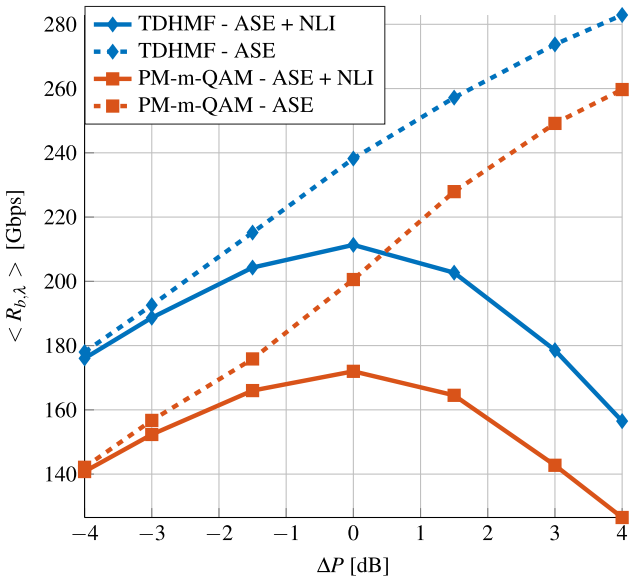

Fig. 5. $\langle R_{b,\lambda} \rangle$ versus ΔP for the two considered modulation strategies. $R_{b,\lambda}$ has been averaged over $N_{\text{MC}} = 2500$ Monte Carlo runs.

As a first analysis, we evaluated the impact of nonlinearities on the average bit rate per LP that the considered network can support. With such a purpose, we set the transmitted power per channel on each link P_{ch} to

$$P_{\text{ch}} = P_{\text{ch,opt}} + \Delta P\,[\text{dBm}], \tag{5}$$

with $\Delta P \in [-4, +4]$dB. Each Monte Carlo analysis was performed either considering or neglecting the effect of NLI by setting η to zero in Eq. (2). As far as the routing policy is concerned, k_{MAX} was set to 1. Figure 5 reports the mean value of the average bit rate per LP $\langle R_{b,\lambda} \rangle$ versus ΔP for each of the two modulation strategies, both considering and neglecting NLI. The pure-format curves display $\langle R_{b,\lambda} \rangle = 172$ Gbps at optimal launch power, while TDHMF allows for the reaching of $\langle R_{b,\lambda} \rangle = 211$ Gbps, as already shown in Fig. 3, showing a 23% advantage at the selected pre-FEC BER of $4 \cdot 10^{-3}$. Using a more powerful FEC would probably increase the mean average bit rate per LP for both TDHMF and pure formats, but the general result, i.e., that TDHMF outperforms flex PM-m-QAM, would still hold. Such noteworthy improvement is enabled by TDHMFs, allowing for a better exploitation of OSNR available on LPs—traded off, however, by an increased complexity of the digital signal processing (DSP) electronics of the transceivers and thus increased capital expenditure for node equipment. Although elastic, the pure-format approach allows for a poor granularity in OSNR versus bpS since, for instance, an approximate 6 dB OSNR increase is required to move from, say, PM-QPSK to PM-16-QAM [29]. TDHMFs allow for the overcoming of such a limitation, thus supporting a relevant performance improvement at a network level.

Always referring to Fig. 5, it can be noted that neglecting NLI $\langle R_{b,\lambda} \rangle$ is overestimated of 13% and 16% at optimal power when considering TDHMF or pure formats,

respectively. In both cases, the error increases if we move away from the optimal power: 27% overestimation for TDHMF and 38% for PM-m-QAM at $P_{ch} = P_{ch,opt} + 1$ dB.

In addition to this type of analysis, to further compare the considered modulation strategies, we have estimated how varying the routing policy characteristics affects network performances. With such an objective, we have varied the parameter k_{MAX}, and thus the number of ranked routes between two nodes that can be considered suitable during the routing and allocation process of the SNAP algorithm, from 1 up to 30. As depicted in Fig. 6, a decrease in the average $R_{b,\lambda}$ at optimal launch power and an increase in its variance take place for increasing k_{MAX}. This behavior can be explained by considering that, as k_{MAX} increases, several paths with nonmaximum QoT will be considered suitable during the RWA process, thus reducing the average OSNR per LP and the corresponding average bit rate per LP as well. Moreover, increasing k_{MAX} enlarges the set of possible paths between node pairs. This provides more candidate paths for demand allocation, thus reducing the blocking ratio and expanding the variability of the RWA outcomes between different Monte Carlo runs. Hence, the variance of $R_{b,\lambda}$ increases with k_{MAX}. Finally, referring to Fig. 6, it can be remarked that the performance advantage of TDHMF with respect to PM-m-QAM formats is independent of k_{MAX}, remaining constant at around 23%.

Finally, in order to show the capabilities of the SNAP algorithm, we report some results related to the average network blocking and link congestions in order to highlight possible critical aspects of the considered pan-European network topology. Figure 7 depicts the average network blocking, i.e., the ratio between the number of blocked LP demands and the total number of LP demands averaged over the set N_{MC} of Monte Carlo runs versus k_{MAX}. Enlarging the set of candidate paths between node pairs allows us to improve the number of allocated demands,

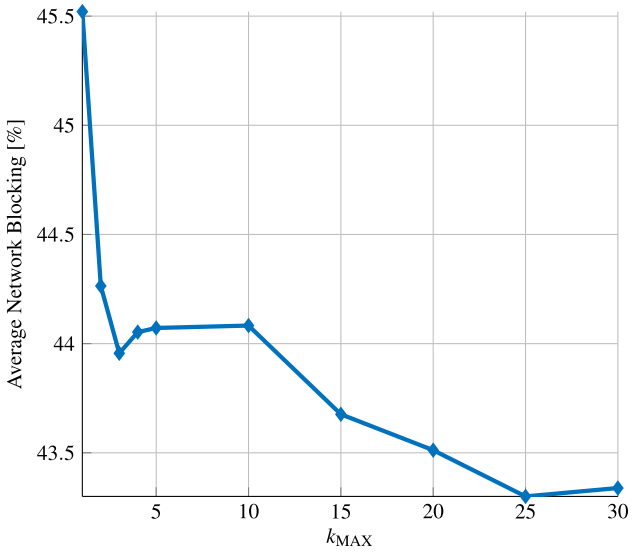

Fig. 7. Average network blocking versus k_{MAX} for TDHMF and PM-m-QAM modulation formats. LOGO strategy has been considered.

but such improvement is only of the order of 2% when moving from $k_{MAX} = 1$ to $k_{MAX} = 30$. This minor improvement is due to the fact that lower QoT paths between node pairs share fiber links with higher QoT paths. As soon as any of these shared fiber links are saturated, it will not be possible to allocate any additional demand on any path that will use these fiber links, thus losing the advantage of considering lower QoT paths.

Figure 8 shows the average link saturation percentage of each link for each considered value of k_{MAX}. This metric is computed by considering the average, over N_{MC} Monte Carlo runs, of the ratio between the number of

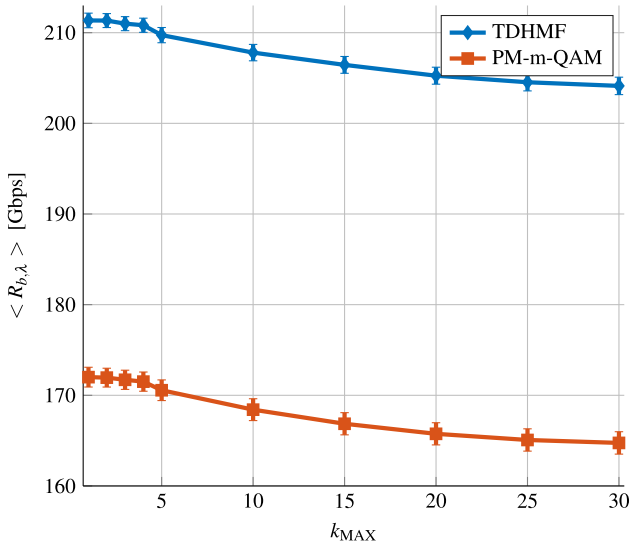

Fig. 6. Average $R_{b,\lambda}$ versus k_{MAX} for TDHMF and PM-m-QAM modulation formats. LOGO strategy has been considered. The $\pm\sigma$ intervals are also shown.

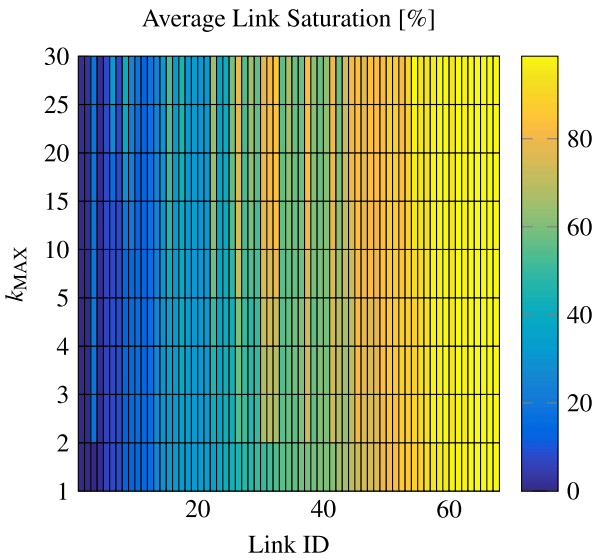

Fig. 8. Average percentage of used wavelengths for each link versus k_{MAX}.

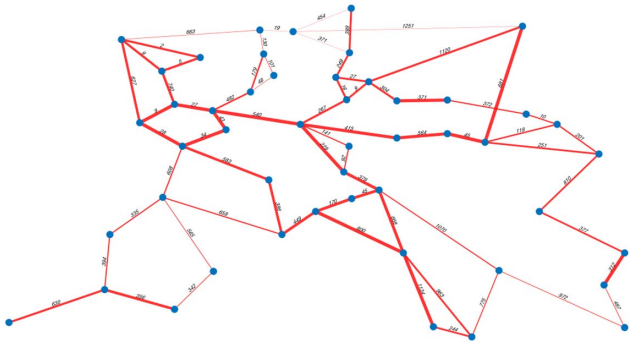

Fig. 9. Pictorial representation of link saturation in the network for $k_{MAX} = 1$. Ticker links correspond to more saturated links. Edge labels represent the link length in km.

allocated wavelengths and the total number of wavelength N_{ch} for each link of the topology. Link indexes are sorted according to the value of the first row, $k_{MAX} = 1$, to improve the quality of the figure.

Figure 9 depicts the link saturation value in the topology: the thicker the edges, the more saturated the links. Comparing Figs. 2 and 9, it can be noted that the longest links are less saturated. This is reasonable, since such links introduce larger IOSNR penalty and therefore are not favorable from the point of view of QoT-based routing. For this reason, in only a few cases long links belong to the best QoT paths, and therefore their available wavelengths are not used. Such a situation could, however, be improved by considering different RWA algorithms aimed at minimizing network blocking.

Referring to Fig. 8, it is possible to notice that many links have an average saturation that is independent of k_{MAX}. This is true especially with links with average saturation greater than or equal to 60%. Less-saturated links may display larger variations. Figure 10 represents the average link saturation percentage, averaged over the set of fiber links, versus k_{MAX}. It can be noted that enlarging k_{MAX} guarantees an improvement in the average saturation of links. However, this gain is relevant up to $k_{MAX} = 5$, since the link saturation grows from 55% to 59%. As k_{MAX} exceeds 5, the steepness of the average link saturation decreases and the metric bottoms out at around 62%.

Thanks to Fig. 8, it is possible to identify *at a glance* all congested links and consequently consider the option to light up available dark fiber pairs on these links, thus planning SDM upgrades on the network. Afterward, to evaluate the benefit of the considered SDM solution, e.g., the decrease of the average network blocking, the topology can be updated to consider new fiber pairs and the SNAP algorithm can be used once again to evaluate statistics of network performance. Figure 8 can also be used to identify poorly used links (blue columns) and tackle inefficiencies in the RWA process. In particular, some links may be scarcely utilized due to the large IOSNR degradation that they introduce, thus being continuously discarded by the QoT-based routing algorithm. Thanks to the results of the SNAP algorithm, these critical links can be easily

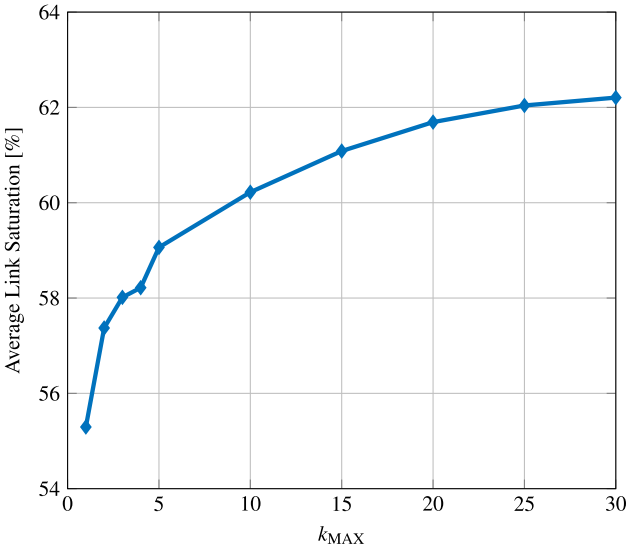

Fig. 10. Mean percentage of used wavelengths averaged over all links versus k_{MAX} for TDHMF and PM-m-QAM modulation formats. LOGO strategy has been considered.

recognized and general solutions to improve this situation, e.g., the introduction of Raman amplification [30] on large Δ_{IOSNR} links, can once again be statistically tested through SNAP. The same process can be repeated to evaluate other types of network criticalities and propose solutions to them, whose effectiveness can then be evaluated statistically through SNAP.

VI. Conclusions

In this paper, we carried out a comparison of flexible-rate transponder technologies in a fixed grid network scenario. Two approaches have been considered: elastic transponders based on either pure PM-m-QAM modulation formats or TDHMFs. To perform such analysis, a novel Monte-Carlo-based network-analysis algorithm called SNAP has been proposed and used to perform the analysis on a LOGO pan-European network scenario. Applying SNAP, we showed that the statistics of the average bit rate per lightpath is Gaussian-distributed with respect to the lightpath demands and allocation. Consequently, it can be used as a figure to estimate the merit of different physical layer solutions at the networking level.

SNAP was also used to demonstrate the impact of NLI on maximum network performance and to show how TDHMFs outperform pure formats, allowing a 23% improvement at the selected pre-FEC BER of $4 \cdot 10^{-3}$ in terms of average bit rate per lightpath, independently of the RWA characteristics in the considered DWDM fixed-grid network. Even by using a more powerful FEC, TDHMF would still outperform PM-m-QAM, but further analyses are required to derive the exact performance gain. Showing results obtained by *turning off* the fiber nonlinearities, we demonstrated how the inclusion of a detailed model for the physical layer is essential in order to properly

address network performance. Possible applications of the proposed methodology have also been shown by highlighting critically congested links in the network.

Given the tight requirements imposed by network operators, the elastic paradigm will be surely implemented in various optical network technologies. Thus, we believe that further analysis will be needed in the near future to fully understand potentialities and criticalities of such technologies. In this context, the SNAP algorithm will be a useful tool for network performance assessment since it allows for the precise appraisal of different aspects of optical networks in a general way.

Acknowledgment

The authors would like to thank M. Schiano and M. Quagliotti of Telecom Italia Lab for providing the pan-European network model and for the helpful suggestions, Professor E. Leonardi for the fruitful discussions, and the reviewers for the useful comments that improved the quality of this paper.

References

[1] Cisco, "Cisco visual networking index: Forecast and methodology, 2014–2019," Tech. Rep., 2014.

[2] G. Wellbrock and T. Xia, "How will optical transport deal with future network traffic growth?" in *European Conf. on Optical Communication (ECOC)*, Sept. 2014, pp. 1–3.

[3] X. Zhou, L. Nelson, and P. Magill, "Rate-adaptable optics for next generation long-haul transport networks," *IEEE Commun. Mag.*, vol. 51, no. 3, pp. 41–49, Mar. 2013.

[4] V. Curri, A. Carena, P. Poggiolini, R. Cigliutti, F. Forghieri, C. R. Fludger, and T. Kupfer, "Time-division hybrid modulation formats: Tx operation strategies and countermeasures to nonlinear propagation," in *Optical Fiber Communication Conf.*, San Francisco, CA, 2014, paper Tu3A.2.

[5] F. P. Guiomar, R. Li, A. Carena, C. R. S. Fludger, and V. Curri, "Hybrid modulation formats enabling elastic fixed-grid optical networks," *J. Opt. Commun. Netw.*, to be published.

[6] H. Dai, Y. Li, and G. Shen, "Explore maximal potential capacity of WDM optical networks using time domain hybrid modulation technique," *J. Lightwave Technol.*, vol. 33, no. 18, pp. 3815–3826, Sept. 2015.

[7] G. Shen, S. Bose, T. Cheng, C. Lu, and T. Chai, "Efficient heuristic algorithms for light-path routing and wavelength assignment in WDM networks under dynamically varying loads," *Comput. Commun.*, vol. 24, no. 3–4, pp. 364–373, 2001.

[8] M. Cantono, R. Gaudino, and V. Curri, "Data-rate figure of merit for physical layer in fixed-grid reconfigurable optical networks," in *Optical Fiber Communication Conf.*, Anaheim, CA, 2016, paper Tu3F.3.

[9] P. Poggiolini, G. Bosco, A. Carena, R. Cigliutti, V. Curri, F. Forghieri, R. Pastorelli, and S. Piciaccia, "The LOGON strategy for low-complexity control plane implementation in new-generation flexible networks," in *Optical Fiber Communication Conf. and the Nat. Fiber Optic Engineers Conf.*, Anaheim, CA, 2013, paper OW1H.3.

[10] R. Pastorelli, G. Bosco, S. Piciaccia, and F. Forghieri, "Network planning strategies for next-generation flexible optical networks," *J. Opt. Commun. Netw.*, vol. 7, no. 3, pp. A511–A525, Mar. 2015.

[11] P. Poggiolini, G. Bosco, A. Carena, V. Curri, Y. Jiang, and F. Forghieri, "The GN-model of fiber non-linear propagation and its applications," *J. Lightwave Technol.*, vol. 32, no. 4, pp. 694–721, Feb. 2014.

[12] V. Curri, A. Carena, A. Arduino, G. Bosco, P. Poggiolini, A. Nespola, and F. Forghieri, "Design strategies and merit of system parameters for uniform uncompensated links supporting Nyquist-WDM transmission," *J. Lightwave Technol.*, vol. 33, no. 18, pp. 3921–3932, Sept. 2015.

[13] L. Zhang, W. Lu, X. Zhou, and Z. Zhu, "Dynamic RMSA in spectrum-sliced elastic optical networks for high-throughput service provisioning," in *Int. Conf. on Computing, Networking and Communications (ICNC)*, San Diego, CA, Jan. 2013, pp. 380–384.

[14] P. Wright, A. Lord, and S. Nicholas, "Comparison of optical spectrum utilization between flexgrid and fixed grid on a real network topology," in *Optical Fiber Communication Conf. and Exposition and the Nat. Fiber Optic Engineers Conf. (OFC/NFOEC)*, Los Angeles, CA, Mar. 2012, pp. 1–3.

[15] A. Carena, V. Curri, G. Bosco, P. Poggiolini, and F. Forghieri, "Modeling of the impact of nonlinear propagation effects in uncompensated optical coherent transmission links," *J. Lightwave Technol.*, vol. 30, no. 10, pp. 1524–1539, May 2012.

[16] A. Bononi, P. Serena, N. Rossi, E. Grellier, and F. Vacondio, "Modeling nonlinearity in coherent transmissions with dominant intrachannel-four-wave-mixing," *Opt. Express*, vol. 20, no. 7, pp. 7777–7791, Mar. 2012.

[17] A. Mecozzi and R. Essiambre, "Nonlinear Shannon limit in pseudolinear coherent systems," *J. Lightwave Technol.*, vol. 30, no. 12, pp. 2011–2024, June 2012.

[18] M. Secondini and E. Forestieri, "Analytical fiber-optic channel model in the presence of cross-phase modulation," *IEEE Photon. Technol. Lett.*, vol. 24, no. 22, pp. 2016–2019, Nov. 2012.

[19] P. Johannisson and M. Karlsson, "Perturbation analysis of nonlinear propagation in a strongly dispersive optical communication system," *J. Lightwave Technol.*, vol. 31, no. 8, pp. 1273–1282, Apr. 2013.

[20] R. Dar, M. Feder, A. Mecozzi, and M. Shtaif, "Properties of nonlinear noise in long, dispersion-uncompensated fiber links," *Opt. Express*, vol. 21, no. 22, pp. 25685–25699, Nov. 2013.

[21] P. Serena and A. Bononi, "An alternative approach to the Gaussian noise model and its system implications," *J. Lightwave Technol.*, vol. 31, no. 22, pp. 3489–3499, Nov. 2013.

[22] M. Secondini, E. Forestieri, and G. Prati, "Achievable information rate in nonlinear WDM fiber-optic systems with arbitrary modulation formats and dispersion maps," *J. Lightwave Technol.*, vol. 31, no. 23, pp. 3839–3852, Dec. 2013.

[23] R. Dar, M. Feder, A. Mecozzi, and M. Shtaif, "Accumulation of nonlinear interference noise in fiber-optic systems," *Opt. Express*, vol. 22, no. 12, pp. 14199–14211, June 2014.

[24] P. Roorda and B. Collings, "Evolution to colorless and directionless ROADM architectures," in *Optical Fiber Communication Conf. and the Nat. Fiber Optic Engineers Conf. (OFC/NFOEC)*, San Diego, CA, Feb. 2008, pp. 1–3.

[25] Y. Li, L. Gao, G. Shen, and L. Peng, "Impact of ROADM colorless, directionless, and contentionless (CDC) features on optical network performance," *J. Opt. Commun. Netw.*, vol. 4, no. 11, pp. B58–B67, Nov. 2012.

[26] A. Devarajan, K. Sandesha, R. Gowrishankar, B. Kishore, G. Prasanna, R. Johnson, and P. Voruganti, "Colorless, directionless and contentionless multi-degree ROADM architecture for mesh optical networks," in *2nd Int. Conf. on*

Communication Systems and Networks (COMSNETS), Bangalore, Jan. 2010, pp. 1–10.

[27] IDEALIST [Online]. Available: http://www.ict-idealist.eu/.

[28] M. Nölle, F. Frey, R. Elschner, C. Schmidt-Langhorst, A. Napoli, and C. Schubert, "Performance comparison of different 8QAM constellations for the use in flexible optical networks," in *Optical Fiber Communications Conf. and Exhibition (OFC)*, San Francisco, CA, Mar. 2014, pp. 1–3.

[29] D. J. Ives, P. Bayvel, and S. J. Savory, "Assessment of options for utilizing SNR margin to increase network data throughput," in *Optical Fiber Communications Conf. and Exhibition (OFC)*, Los Angeles, CA, Mar. 2015, pp. 1–3.

[30] V. Curri and A. Carena, "Merit of Raman pumping in uniform and uncompensated links supporting NYWDM transmission," *J. Lightwave Technol.*, vol. 34, no. 2, pp. 554–565, 2016.